

Lanthanide Contraction within a Series of
Asymmetric Dinuclear [Ln₂] ComplexesDavid Aguilà,^[a] Leoní A. Barrios,^[a] Verónica Velasco,^[a] Leticia Arnedo,^[a]
Núria Aliaga-Alcalde,^[b, c] Melita Menelaou,^[a, d] Simon J. Teat,^[e] Olivier Roubeau,^[f]
Fernando Luis,^[f] and Guillem Aromí*^[a]

Abstract: A complete isostructural series of dinuclear asymmetric lanthanide complexes has been synthesized by using the ligand 6-[3-oxo-3-(2-hydroxyphenyl)propionyl]pyridine-2-carboxylic acid (H₃L). All complexes have the formula [Ln₂(HL)₂(H₂L)(NO₃)(py)(H₂O)] (Ln = La (1), Ce (2), Pr (3), Nd (4), Sm (5), Eu (6), Gd (7), Tb (8), Dy (9), Ho (10), Er (11), Tm (12), Yb (13), Lu (14), Y (15); py = pyridine). Complexes of La to Yb and Y have been crystallographically characterized to reveal that the two metal ions are encapsulated within two distinct coordination environments of differing size. Whereas one site maintains the coordination number (nine) through the whole series, the other one increases from nine to ten owing to a change in

the coordination mode of an NO₃⁻ ligand. This series offers a unique opportunity to study in detail the lanthanide contraction within complexes of more than one metal. This analysis shows that various representative parameters proportional to this contraction follow a quadratic decay as a function of the number *n* of f electrons. Slater's model for the atomic radii has been used to extract, from these decays, the shielding constant of 4f electrons. The average of O...O distances within the coordination polyhedra shared by both metals and of the

Ln...Ln separations follow also a quadratic decay, therefore showing that such dependence holds also for parameters that receive the contribution of two lanthanide ions simultaneously. The magnetic behavior has been studied for all nondiamagnetic complexes. It reveals the effect of the spin-orbit coupling and a weak antiferromagnetic interaction between both metals. Photoluminescent studies of all the complexes in the series reveal a single broad emission band in the visible region, which is related to the coordinated ligand. On the other hand, the Nd, Er, and Yb complexes show features in the near-IR region due to metal-based transitions.

Keywords: contraction • lanthanides • luminescence • magnetic properties • X-ray diffraction

Introduction

The coordination chemistry of lanthanides is relevant to a wide variety of fields of science and technology as a result of the properties that arise from the peculiar electronic structure of these metals. Among the most attractive phenomena associated with 4f elements are these of photonic nature.^[1-6] These elements are also of interest for their mag-

netic properties,^[7] in many respects more relevant than 3d metals^[8] in their potential role as part of molecular information storage devices.^[9-14] In contrast to the richness and plasticity of their magnetic and optical properties, the metals of the 4f period exhibit a more regular chemical behavior, in part owing to the lack of strong consequences from small differences in crystal-field effects. This has stimulated synthetic chemists to face the challenge of constructing more or

[a] D. Aguilà, Dr. L. A. Barrios, V. Velasco, L. Arnedo, Dr. M. Menelaou, Dr. G. Aromí
Departament de Química Inorgànica
Universitat de Barcelona
Diagonal 645, 08028 Barcelona (Spain)
E-mail: guillem.aromi@qi.ub.es

[b] Dr. N. Aliaga-Alcalde
Institució Catalana de Recerca i Estudis Avançats (ICREA)
Departament de Química Inorgànica
Universitat de Barcelona
Diagonal 645, 08028 Barcelona (Spain)

[c] Dr. N. Aliaga-Alcalde
Current address: ICREA—Institut de Ciència de Materials de Barcelona (ICMAB-CSIC), Campus de la UAB
08193 Bellaterra (Spain)

[d] Dr. M. Menelaou
Current address: Department of General and Inorganic Chemistry
School of Chemistry, Aristotle University of Thessaloniki
54124 Thessaloniki (Greece)

[e] Dr. S. J. Teat
Advanced Light Source, Berkeley Laboratory
1 Cyclotron Road, Berkeley, CA 94720 (USA)

[f] Dr. O. Roubeau, Dr. F. Luis
Instituto de Ciencia de Materiales de Aragón (ICMA)
CSIC and Universidad de Zaragoza
Plaza San Francisco s/n, 50009 Zaragoza (Spain)

Supporting information for this article is available on the WWW under <http://dx.doi.org/10.1002/chem.201204451>.

less comprehensive (quasi)isostructural series of complexes that contain lanthanides. From the analysis of these series emerges the conclusion that whenever differences in chemical reactivity occur, these mainly arise from the systematic decrease in ionic radius that takes place when increasing the atomic number throughout the series, a phenomenon that is termed lanthanide contraction.^[15] Very often, the result is a decrease in coordination number (CN) as the ionic radius shrinks (most frequently, the CN ranges from 7 to 10).^[16,17] Flexible bridging ligands often lead to polymeric arrangements of lanthanides (1D, 2D, or 3D), with dramatic structural differences upon going from metal to metal as a result of the slight changes in size.^[18–20] In very few of the rather complete series reported do all the complexes exhibit the exact same molecular structure and space group. This occurs almost exclusively with multidentate ligands that exhibit enough flexibility to accommodate ions of different sizes while encapsulating them within a fixed coordination environment.^[21–24] The seeming exception of the isostructural series of nonacoordinated complexes $[\text{Ln}(\text{H}_2\text{O})_9](\text{CF}_3\text{SO}_3)_3$ ^[25] was demonstrated by detailed solid and solution extended X-ray absorption fine structure (EXAFS) and crystallographic studies to exhibit effective changes in coordination number that result from varying partial occupancies of some coordination sites.^[26] In the special cases that are isostructural, it is possible to examine the consequences of the lanthanide contraction throughout the series. An accurate analysis of the Ln–O distances in one such family allowed us to conclude that this contraction follows a quadratic decay as a function of the number of *f* electrons.^[27] Such a behavior was later shown^[24] to follow from Slater's model for calculating atomic radii.^[28,29] For series of complexes that contain different types of O-donor atoms bound to the metal, a smooth behavior is obtained if the ensemble of the Ln–O distances is analyzed as a whole (e.g., by observing the decay of the sum of Ln–O distances for each complex). Other parameters directly affected by the contraction were found to exhibit the same quadratic decay, such as the sum of the O–O distances featured by the coordination polyhedron (i.e., the sum of the lengths of the edges).^[24] The literature contains some series of dinuclear complexes of lanthanides, which usually contain fewer members.^[30–33] From the point of view of the single-ion structure, such series should not be much more informative than mononuclear ones, considering that in these complexes both metals are structurally equal. It would be interesting to analyze individually and collectively the effect of lanthanide contraction of systems that contain more than one noncrystallographically equivalent metal. We report here an extensive quasi-isostructural series of dinuclear lanthanide complexes with formulae $[\text{Ln}_2(\text{HL})_2(\text{H}_2\text{L})(\text{NO}_3)(\text{py})(\text{H}_2\text{O})]$ (py = pyridine; Ln = La (1), Ce (2), Pr (3), Nd (4), Sm (5), Eu (6), Gd (7), Tb (8), Dy (9), Ho (10), Er (11), Tm (12), Yb (13), Y (15); H_3L = 6-[3-oxo-3-(2-hydroxyphenyl)propionyl]pyridine-2-carboxylic acid) in which both metals from each molecule exhibit distinct coordination environments (see Figure 1). The analogue of the complex containing Lu (14) has also been pre-

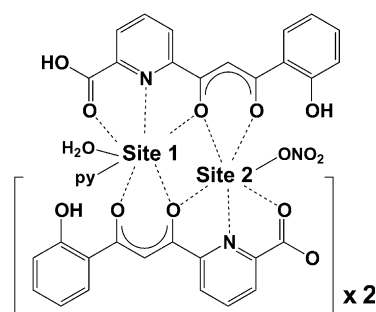


Figure 1. Schematic representation of the structure of complexes $[\text{Ln}_2(\text{HL})_2(\text{H}_2\text{L})(\text{NO}_3)(\text{py})(\text{H}_2\text{O})]$ (1 to 15), emphasizing the difference between coordinating sites 1 (CN = 9) and 2 (CN = 9 if NO_3^- is monodentate or 10 if it is bidentate).

pared, although its structure is not available. In these compounds, one of the sites maintains the same nine-coordinate environment throughout the series, whereas the other site features a transition from CN = 10 for the larger metals to CN = 9 for the smaller ions, facilitated by a transition from chelating to monodentate of a nitrate ligand. This series provides a unique opportunity to investigate the structural contraction of lanthanides on molecules that simultaneously feature both situations, that is, conservation and variation of CN throughout the series. Such analysis is presented in this paper together with a brief description of magnetic and optical properties.

Results and Discussion

Synthesis: The ligand H_3L was obtained by the Claisen condensation of 2-hydroxyacetophenone and the asymmetric species 6-(methoxycarbonyl)pyridine-2-carboxylic acid, as previously reported.^[34] This ligand was previously used in our group for the synthesis of asymmetric dinuclear complexes with the metals from the central segment of the lanthanide series $[\text{Gd}_2(\text{HL})_2(\text{H}_2\text{L})\text{Cl}(\text{py})(\text{H}_2\text{O})]$ (16), $[\text{Tb}_2(\text{HL})_2(\text{H}_2\text{L})\text{Cl}(\text{py})_2]$ (17), and $[\text{Eu}_2(\text{HL})_2(\text{H}_2\text{L})(\text{NO}_3)(\text{py})(\text{H}_2\text{O})]$ (6a) with almost identical structure (see below). Asymmetric dinuclear complexes of 4f metals are extremely less frequent than symmetric ones. These species have been proposed as possible realizations of molecular-spin-based quantum gates,^[35] and in fact, complex 17 was shown to fulfill many of the basic requirements.^[36] The structural consistency in this peculiar reaction system appeared as a good opportunity to generate an analogous sequence for a systematic study on the lanthanide series. This structural type is of interest because it contains metals in two distinct coordination environments, one that appears to accommodate larger metals than the other (Figure 1 and see below). Thus, one outstanding question was whether or not the scaffold formed by the various ligands of this molecular arrangement would be capable of encapsulating any of the 4f homometallic pairs, independently of their varying sizes. For this purpose, NO_3^- was chosen as the participant coun-

terion. Thus, the stoichiometric amounts of H₃L and the corresponding Ln(NO₃)₃ salt were stirred in pyridine and the resulting solutions yielded, upon diffusion of diethyl ether or toluene, crystals of the pertinent [Ln₂(HL)₂(H₂L)(NO₃)(py)(H₂O)] complex (Ln = Ce (**2**), Pr (**3**), Nd (**4**), Sm (**5**), Eu (**6**), Gd (**7**), Tb (**8**), Dy (**9**), Ho (**10**), Er (**11**), Tm (**12**), Y (**15**)). The identity of all the molecules was established by single-crystal X-ray diffraction (see below), and their composition was consistent with results from microanalysis, mass spectrometry, and bulk magnetization measurements. All complexes exhibited virtually the same IR spectrum (see the Supporting Information and Figure S1 therein). All attempts to obtain crystals of the analogues with La (**1**), Yb (**13**), and Lu (**14**) by using the above reaction failed. However, yellow crystals of [La₂(HL)₂(H₂L)(NO₃)(py)(H₂O)] (**1**) and [Yb₂(HL)₂(H₂L)(NO₃)(py)(H₂O)] (**13**) were isolated when one and three equivalents, respectively, of HNO₃ was added to the reaction. Since these complexes feature two different deprotonated forms of H₃L (depending on whether or not the carboxylic moiety maintains the proton), it was thought that the presence of a small amount of nitric acid

could affect the formation or crystallization of the complexes, given that these processes coexist with a series of acid–base equilibria. This did not, however, allow us to obtain **15** in crystalline form. Nevertheless, evidence for the identity of the latter complex, as prepared in the conventional manner, was obtained from elemental analysis, IR, and mass spectrometry.

Description of the structures: Complexes **1** to **13** and **15** crystallize in the monoclinic space group *P*2₁/*c*. All compounds exhibit an [Ln₂] molecule in the asymmetric unit in addition to five molecules of pyridine (four in the case of [Y₂], **15**). The compounds differ in the nature of an almost always present additional solvent molecule (or fraction of it) per asymmetric unit, which in most cases is pyridine, but can also be H₂O or Et₂O (see Table 1 and cif files, available from the Cambridge Crystallographic Data Centre; see Experimental Section). All compounds exhibit four asymmetric units in the unit cell and display similar cell parameters (Table 1). Compounds **1** to **13** and **15** are divided into two groups, depending on the coordination mode of the terminal

Table 1. Crystal data and structure refinement for compounds **1–13** and **15**.^[a,b]

	1·5 py	2·6 py	3·6 py	4·6 py	5·5 py·H ₂ O	6·5 py·H ₂ O	7·5 py
<i>T</i> [K]	100	100	100	100	150	100	150
formula	C ₇₅ H ₆₀ La ₂ N ₁₀ O ₁₉	C ₈₀ H ₆₅ Ce ₂ N ₁₁ O ₁₉	C ₈₀ H ₆₅ Nd ₂ O ₁₉ Pr ₂	C ₈₀ H ₆₅ N ₁₁ Nd ₂ O ₁₉	C ₇₅ H ₆₂ N ₁₀ O ₂₀ Sm ₂	C ₇₅ H ₆₂ Eu ₂ N ₁₀ O ₂₀	C ₇₅ H ₆₀ Gd ₂ N ₁₀ O ₁₉
<i>M</i> _r	1683.15	1764.67	1766.25	1772.91	1724.05	1727.27	1719.83
<i>λ</i> [Å]	0.71073	0.7749	0.7749	0.71073	0.7749	0.7749	0.71073
<i>a</i> [Å]	14.9646(7)	14.867(2)	14.907(3)	14.514(1)	14.894(5)	14.813(3)	14.2665(11)
<i>b</i> [Å]	15.6293(7)	15.560(2)	15.574(3)	15.772(1)	15.586(5)	15.637(4)	15.4250(8)
<i>c</i> [Å]	33.8889(14)	34.323(3)	34.009(6)	35.797(3)	32.554(8)	32.594(6)	35.006(3)
<i>β</i> [°]	110.799(2)	110.830(4)	111.316(8)	113.692(4)	111.183(11)	110.806(8)	109.791(7)
<i>V</i> [Å ³]	7409.6(6)	7421.0(15)	7355(2)	7503.8(9)	7046(4)	7057(3)	7248.4(9)
<i>ρ</i> [g cm ⁻³]	1.509	1.579	1.595	1.569	1.625	1.626	1.576
reflns	15134	18408	22491	16524	11763	19770	12317
params	1010	1077	1063	955	964	970	985
restraints	302	234	454	242	272	182	430
<i>R</i> _{int}	0.0832	0.0586	0.0479	0.0687	0.0561	0.0508	0.1501
<i>R</i> ₁ ^[c]	0.0518	0.0605	0.0536	0.0657	0.0907	0.0729	0.1172
<i>wR</i> ₂ ^[d]	0.1295	0.1480	0.1364	0.1607	0.2535	0.1642	0.2290
<i>S</i>	1.029	1.134	1.160	1.079	1.216	1.257	1.172

	8·5 py	9·5 py	10·5 py	11·5 py	12·5 py·Et ₂ O	13·6 py	15·4 py
<i>T</i> [K]	100	150	150	100	150	100	100
formula	C ₇₅ H ₆₀ N ₁₀ O ₁₉ Tb ₂	C ₇₅ H ₆₀ Dy ₂ N ₁₀ O ₁₉	C ₇₅ H ₆₀ Ho ₂ N ₁₀ O ₁₉	C ₇₅ H ₆₀ Er ₂ N ₁₀ O ₁₉	C ₇₀ H ₇₀ N ₁₀ O ₂₀ Tm ₂	C ₈₀ H ₆₅ N ₁₁ O ₁₉ Yb ₂	C ₇₀ H ₅₅ N ₉ O ₁₉ Y ₂
<i>M</i> _r	1723.17	1730.33	1735.19	1739.85	1817.31	1830.51	1504.05
<i>λ</i> [Å]	0.7749	0.71073	0.71073	0.7749	0.71073	0.71073	0.7749
<i>a</i> [Å]	14.255(4)	14.3307(10)	14.3450(5)	14.123(2)	14.3231(2)	14.1022(8)	14.108(7)
<i>b</i> [Å]	15.513(4)	15.6882(7)	15.6609(3)	15.400(2)	15.6838(2)	15.3860(8)	15.367(8)
<i>c</i> [Å]	34.078(8)	35.637(2)	35.6109(9)	34.488(3)	35.5024(7)	35.172(2)	34.70(2)
<i>β</i> [°]	110.416(10)	110.910(5)	110.211(2)	110.659(4)	109.857(2)	110.131(4)	110.79(2)
<i>V</i> [Å ³]	7063(3)	7484.4(7)	7507.6(4)	7018.6(15)	7501.1(2)	7165.3(7)	7033(6)
<i>ρ</i> [g cm ⁻³]	1.621	1.536	1.535	1.647	1.609	1.697	1.420
reflns	9440	10619	10634	17299	15325	14547	5953
params	974	955	937	964	1006	1009	901
restraints	359	437	169	116	229	162	561
<i>R</i> _{int}	0.0949	0.1656	0.0955	0.0524	0.1090	0.0907	0.1410
<i>R</i> ₁ ^[c]	0.0912	0.0819	0.0453	0.0608	0.0540	0.0767	0.1376
<i>wR</i> ₂ ^[d]	0.2059	0.1646	0.0938	0.1472	0.1135	0.2076	0.3382
<i>S</i>	1.090	0.960	0.902	1.067	0.982	1.058	1.086

[a] The structure of compound **6a** has been reported previously.^[33] [b] For all compounds, the crystal system is monoclinic, the space group is *P*2₁/*c*, and *Z* = 4. [c] *R*₁ = $\sum ||F_o| - |F_c|| / \sum |F_o|$, for *I* > 2σ(*I*). [d] *wR*₂ = $[\sum (w(F_o^2 - F_c^2))^2 / \sum (w(F_o^2))^2]^{1/2}$ for all data.

nitrate ligand of the $[\text{Ln}_2(\text{HL})_2(\text{H}_2\text{L})(\text{NO}_3)(\text{py})(\text{H}_2\text{O})]$ molecule. For the group of lighter metals (from La to Eu (hereafter referred to as “group I”), **1** to **6**), the ligand NO_3^- is didentate and chelating, whereas for the rest of metals (including Y and presumably Lu (hereafter referred to as “group II”), **7** to **13**, **15**, and most likely **14**), this donor acts in a monodentate fashion. Figure 2 shows one representative molecule for each of both types, and selected structural pa-

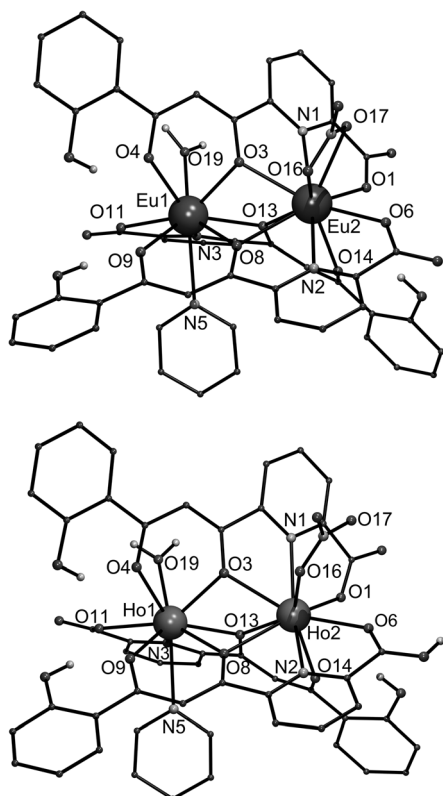


Figure 2. Povray molecular structure of $[\text{Eu}_2(\text{HL})_2(\text{H}_2\text{L})(\text{NO}_3)(\text{py})(\text{H}_2\text{O})]$ (**6**, top) and $[\text{Ho}_2(\text{HL})_2(\text{H}_2\text{L})(\text{NO}_3)(\text{py})(\text{H}_2\text{O})]$ (**9**, bottom), representing complexes of groups I and II, respectively (see text). Only crystallographically found hydrogen atoms on O carriers are represented.

rameters are listed in Table S1 in the Supporting Information. The complex $[\text{Ln}_2(\text{HL})_2(\text{H}_2\text{L})(\text{NO}_3)(\text{py})(\text{H}_2\text{O})]$ in all compounds is a chiral species, which is accompanied by its enantiomeric counterpart in the unit cell as generated by symmetry. This molecule comprises two Ln^{III} metals linked by three H_3L ligands in different degrees of deprotonation, one as H_2L^- and two as HL^{2-} . Thus each of these ligands loses one proton from the β -diketone group upon coordination, whereas the carboxylic H^+ is also absent from two of them. The $-\text{COOH}$ proton that remains in the H_2L^- moiety was either determined crystallographically or inferred from the establishment of hydrogen bonds with either one or two lattice pyridine molecules. Each deprotonated ligand chelates both metals through its dipicolinate-like and β -diketonate pockets, respectively, and bridges them with the O atom that is common to both chelating moieties (Figure 1).

The asymmetry of H_3L causes both metals to be accommodated in completely different coordination environments. One of the sites (site 1) comprises one dipicolinate “ONO” pocket and two β -diketonate “OO” units, in addition to one molecule of pyridine and one of H_2O , which complete a coordination environment with $\text{CN}=9$. The protons of the latter ligand were found to form hydrogen bonds with lattice pyridine molecules. The other location (site 2) is formed by two of the “ONO” units and one of the “OO” pockets, whereas a didentate (group I) or monodentate (group II) NO_3^- ligand completes nona- or decacoordination, respectively (Figure 2). The decrease in the coordination number as a result of the lanthanide contraction when no restrictions prevent it is an established fact.^[15,19,37] In the current series, the transition occurs between the elements Eu and Gd. However, the metals that mark the limits between groups vary from system to system. It must also be emphasized that our previously reported^[34] polymorph of $[\text{Eu}_2(\text{HL})_2(\text{H}_2\text{L})(\text{NO}_3)(\text{py})(\text{H}_2\text{O})]$ (**6a**) exhibits monodentate NO_3^- , contrary to what has been observed from the structure of the complex reported here, **6**, in which NO_3^- is η^2 . This means that for this metal, both forms, **6** and **6a**, are very similar in stability. This sort of “bistability” near the transition between two structural types has been observed already for other Ln series.^[37] The heterogeneity of the ligand set in this family causes the irregularity of the coordination polyhedra around the metals. Continuous shape measures (CSHMs)^[38,39] have been performed to elucidate the closest ideal figures approximated by these polyhedra (see Figure S2 and Tables S2 and S3 in the Supporting Information for a complete set of distances to several model geometries). For site 1, the geometries have been found to approximate to either a spherical capped antiprism (C_{4v} symmetry; compounds **1** to **8**, **11**, **13**, and **15**) or a spherical tricapped trigonal prism (D_{3h} symmetry; compounds **9**, **10**, and **12**). Site 2 is more irregular in nature since the distances of the coordination figures of this site to any ideal polyhedron are always more than four times larger than any of the best values observed for site 1. Thus, for compounds of group I (decacoordinate), the closest symmetry to site 2 is always C_{2v} , with a preferred sphenocorona geometry for complexes **2** to **4**, and that of a tetracaehedron for **1**, **5**, and **6**. Site 2 of group II (nonacoordinate, compounds **7** to **13** and **15**) exhibits a closest resemblance to the ideal figure that is termed “muffin”.

Analysis of the lanthanide contraction: Table 2 lists all Ln–X (X=O, N) bond lengths for complexes **1** to **13** and **15**. It can be seen that these distances follow the trend dictated by the lanthanide contraction, that is, with increasing atomic number Z , they decrease, as do the ionic radii of the metals. From previous reports,^[27] it was shown by analyzing the decay of bond lengths that this contraction follows a quadratic decay as a function of the number n of f electrons. Later on,^[24] the polynomial dependence of the lanthanide contraction was associated with the model of Slater that states that the atomic or ionic radii corresponds to the maximum of the radial part, r_{max} , of the outermost orbital of the

Table 2. Ln–X bond lengths and Ln···Ln separations [Å] for compounds **1–13** and **15**.

	La (1)	Ce (2)	Pr (3)	Nd (4)	Sm (5)	Eu (6)	Gd (7)
$d_{\text{Ln1-O3}} (\sigma)$	2.493(3)	2.467(4)	2.445(3)	2.420(5)	2.422(10)	2.406(5)	2.375(11)
$d_{\text{Ln1-O4}} (\sigma)$	2.524(3)	2.513(4)	2.486(3)	2.483(4)	2.466(9)	2.447(5)	2.458(11)
$d_{\text{Ln1-O8}} (\sigma)$	2.541(3)	2.511(3)	2.482(3)	2.469(4)	2.408(9)	2.409(5)	2.416(10)
$d_{\text{Ln1-O9}} (\sigma)$	2.457(3)	2.444(3)	2.419(3)	2.405(4)	2.361(10)	2.352(5)	2.339(11)
$d_{\text{Ln1-O11}} (\sigma)$	2.455(3)	2.428(4)	2.412(3)	2.407(4)	2.388(10)	2.383(5)	2.372(12)
$d_{\text{Ln1-O13}} (\sigma)$	2.532(3)	2.520(3)	2.492(3)	2.488(4)	2.439(9)	2.430(4)	2.465(9)
$d_{\text{Ln1-O19}} (\sigma)$	2.579(3)	2.548(4)	2.545(3)	2.487(5)	2.478(11)	2.453(5)	2.444(12)
$d_{\text{Ln1-N3}} (\sigma)$	2.599(4)	2.581(4)	2.557(4)	2.534(5)	2.500(12)	2.500(6)	2.483(13)
$d_{\text{Ln1-N5}} (\sigma)$	2.786(4)	2.767(5)	2.737(4)	2.741(6)	2.720(14)	2.699(7)	2.700(14)
$d_{\text{Ln2-O1}} (\sigma)$	2.463(3)	2.438(4)	2.416(3)	2.419(5)	2.403(10)	2.390(5)	2.361(11)
$d_{\text{Ln2-O3}} (\sigma)$	2.577(3)	2.548(3)	2.534(3)	2.546(4)	2.468(9)	2.473(4)	2.437(9)
$d_{\text{Ln2-O6}} (\sigma)$	2.485(3)	2.461(4)	2.440(3)	2.435(4)	2.397(9)	2.391(5)	2.393(10)
$d_{\text{Ln2-O8}} (\sigma)$	2.693(3)	2.694(4)	2.671(3)	2.661(4)	2.651(9)	2.637(5)	2.631(10)
$d_{\text{Ln2-O13}} (\sigma)$	2.547(3)	2.517(4)	2.499(3)	2.486(4)	2.437(9)	2.430(5)	2.384(10)
$d_{\text{Ln2-O14}} (\sigma)$	2.503(3)	2.483(4)	2.470(3)	2.427(4)	2.454(9)	2.431(5)	2.373(10)
$d_{\text{Ln2-O16}} (\sigma)$	2.628(4)	2.588(5)	2.581(3)	2.544(5)	2.542(10)	2.519(6)	2.424(12)
$d_{\text{Ln2-O17}} (\sigma)$	2.767(4)	2.869(5)	2.771(4)	2.933(8)	2.674(11)	2.687(6)	–
$d_{\text{Ln2-N1}} (\sigma)$	2.674(4)	2.635(5)	2.630(4)	2.595(6)	2.604(13)	2.581(6)	2.538(13)
$d_{\text{Ln2-N2}} (\sigma)$	2.739(4)	2.736(4)	2.714(3)	2.691(5)	2.656(12)	2.664(6)	2.619(12)
$d_{\text{Ln1-Ln2}} (\sigma)$	3.9590(4)	3.9286(5)	3.8941(6)	3.8814(5)	3.8197(13)	3.8173(8)	3.8038(11)
	Tb (8)	Dy (9)	Ho (10)	Er (11)	Tm (12)	Yb (13)	Y (15)
$d_{\text{Ln1-O3}} (\sigma)$	2.374(12)	2.311(11)	2.319(5)	2.339(5)	2.295(5)	2.311(8)	2.269(17)
$d_{\text{Ln1-O4}} (\sigma)$	2.445(11)	2.435(8)	2.407(5)	2.415(5)	2.386(4)	2.400(7)	2.402(15)
$d_{\text{Ln1-O8}} (\sigma)$	2.383(11)	2.378(8)	2.369(5)	2.358(4)	2.349(4)	2.351(7)	2.346(14)
$d_{\text{Ln1-O9}} (\sigma)$	2.336(11)	2.323(9)	2.304(6)	2.290(5)	2.296(4)	2.273(8)	2.282(14)
$d_{\text{Ln1-O11}} (\sigma)$	2.355(12)	2.315(10)	2.328(5)	2.324(5)	2.307(5)	2.305(8)	2.329(15)
$d_{\text{Ln1-O13}} (\sigma)$	2.463(9)	2.455(7)	2.431(4)	2.394(4)	2.414(4)	2.401(7)	2.433(13)
$d_{\text{Ln1-O19}} (\sigma)$	2.416(12)	2.424(10)	2.394(6)	2.381(5)	2.371(5)	2.357(8)	2.383(16)
$d_{\text{Ln1-N3}} (\sigma)$	2.482(13)	2.466(10)	2.447(6)	2.437(6)	2.423(5)	2.419(8)	2.434(18)
$d_{\text{Ln1-N5}} (\sigma)$	2.648(16)	2.682(15)	2.665(7)	2.670(7)	2.664(6)	2.666(11)	2.680(20)
$d_{\text{Ln2-O1}} (\sigma)$	2.375(11)	2.358(9)	2.348(5)	2.339(4)	2.344(5)	2.328(7)	2.313(14)
$d_{\text{Ln2-O3}} (\sigma)$	2.459(10)	2.471(8)	2.451(5)	2.418(4)	2.450(4)	2.399(7)	2.441(14)
$d_{\text{Ln2-O6}} (\sigma)$	2.367(10)	2.359(9)	2.354(5)	2.339(4)	2.342(4)	2.327(7)	2.317(14)
$d_{\text{Ln2-O8}} (\sigma)$	2.630(10)	2.570(9)	2.562(5)	2.603(4)	2.545(4)	2.600(7)	2.618(13)
$d_{\text{Ln2-O13}} (\sigma)$	2.359(10)	2.374(9)	2.365(5)	2.331(5)	2.352(4)	2.304(7)	2.291(15)
$d_{\text{Ln2-O14}} (\sigma)$	2.371(10)	2.340(9)	2.337(5)	2.333(5)	2.323(5)	2.308(7)	2.292(14)
$d_{\text{Ln2-O16}} (\sigma)$	2.399(12)	2.396(11)	2.375(5)	2.380(5)	2.359(5)	2.362(8)	2.392(16)
$d_{\text{Ln2-O17}} (\sigma)$	–	–	–	–	–	–	–
$d_{\text{Ln2-N1}} (\sigma)$	2.492(14)	2.480(12)	2.474(7)	2.483(6)	2.467(6)	2.440(10)	2.460(20)
$d_{\text{Ln2-N2}} (\sigma)$	2.610(13)	2.591(11)	2.581(7)	2.590(5)	2.562(5)	2.554(10)	2.568(18)
$d_{\text{Ln1-Ln2}} (\sigma)$	3.7854(13)	3.7709(9)	3.7570(5)	3.7405(5)	3.7354(4)	3.7245(7)	3.741(4)

corresponding atom or ion. Within this model, the shielding by inner electrons of the nuclear charge experienced by the electrons of the outermost orbital is treated empirically by the use of a screening constant s , which directly affects r_{max} of each Ln^{III} ion. In particular, the influence of adding 4f electrons, known to be the cause of the contraction for their poor screening ability, gives a polynomial expression of r_{max} as a function of n .^[28,29] This translates into the quadratic decay of bond lengths with n . The contraction, however, might affect some bond types differently than others, depending on the constraints imposed by multidentate ligands. Therefore, some authors have studied the decay by considering the combined effect on the totality of bonds ($\sum d_{(\text{Ln-X})}$).^[24] For the sum S_m , of distances of an ensemble of m bonds, Slater's model for the lanthanide contraction yields the relationship [Eq. (1)] in which S_{mL} is the sum of the atomic radii of the m donor atoms considered (assumed to be constant), r_0 and Z_0^* are the ionic radius and effective nuclear charge

(for 5p electrons) of La^{III}, respectively, and k is the screening constant for one 4f electron.

$$S_m(n) = S_{mL} + mr_0 + [mr_0(1-k)/Z_0^*]n + [mr_0(1-k)^2/(Z_0^*)^2]n^2 = a + bn + cn^2 \quad (1)$$

When dealing with the Ln–X distances in the series reported here, we considered that the metal size reduction would have a concerted effect on the overall distance of the (H_{3-x}L)^{-x} ligands to the metals. Thus, for each of the two metals of the dinuclear complex (Ln1 and Ln2), the ensemble of Ln–O distances that involves only these ligands was considered as a whole, excluding the Ln–N bonds for a more homogeneous treatment. Figure 3 shows the variation with n of the sums $\sum_m d(\text{Ln1-O})$ and $\sum_m d(\text{Ln2-O})$ ($m=6$ at both sites) for complexes **1** to **13**. The data could be fit satis-

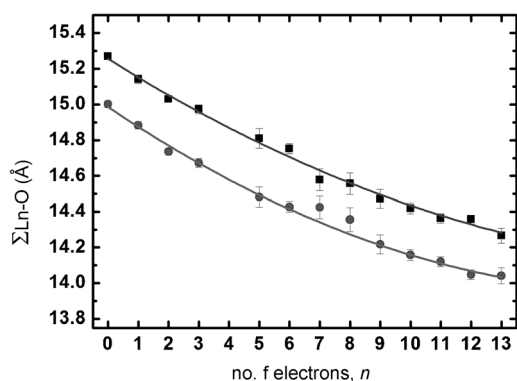


Figure 3. Graph of $\Sigma_m d_{(\text{Ln}-\text{O})}$ versus the number of 4f electrons, n , for sites 1 (circles) and 2 (squares) of complexes **1** to **13**, with $m=6$ (corresponding to the O atoms of the HL^{2-} or H_2L^- ligands). The solid lines are best weighted fits to the quadratic function $\Sigma(n) = a + bn + cn^2$. Best-fit parameters (in the 1/2 format): $a = 14.99(1)/15.26(1)$, $b = -0.114(8)/-0.106(8)$, and $c = 0.0032(6)/0.0024(6)$ with $R^2 = 0.9946/0.9951$.

factorily to a polynomial equation of second order (see the legend of Figure 3 for best-fit coefficients) by employing a weighted regression with a weighting factor of σ^{-2} . From the parameters obtained it is possible to calculate the screening constant k , extracted as $k = 1 + Z_0^*c/b$ from Equation (1), which for $Z_0^* = 15.42^{[28]}$ is found to be equal to 0.57 and 0.65 for Ln1 and Ln2, respectively. These numbers are close to the commonly accepted value of $k = 0.69$ and to the previously determined number for another series of Ln complexes ($k = 0.64$).^[24] The difference in the value of the 4f-electron screening constant obtained for metals in site 1 and site 2 could point, experimentally, to a potential crystal-field effect on the capacity of these electrons to shield the nuclear charge. Another remarkable feature unveiled by this analysis is that one site exhibits systematically a larger $\Sigma_m d_{(\text{Ln}-\text{O})}$ sum than the other (for $m=6$ in both cases), whereas the gap is maintained practically constant throughout the series. This difference in “cavity size” between both sites is undoubtedly the result of the structural constraints imposed by the disposition of ligands within the assembly. Such a “geometric component” imparted by the scaffold of the ligands has an impact on the intercept of the $S(n)$ curves, a . Parameters b and c should almost exclusively be determined by the factors predicted in Slater’s model, as suggested by the fact that they vary little from site 1 to site 2.

The Ln–X distances that involve the H_2O and pyridine ligands in site 1 were also analyzed independently (Figure S3 in the Supporting Information) and produced worse polynomial fits, which is consistent with the proposed fact^[24] that individual bonds might exhibit a more irregular behavior. Another way to evaluate the effect of the contraction is by examining parameters that directly affect the volume of the coordination polyhedron. It was shown previously that the sum of the X···X distances ($\Sigma d_{(\text{X}\cdots\text{X})}$) that corresponds to the edges of this polyhedron in mononuclear complexes also exhibits a quadratic decay with n .^[24] In the series **1** to **13**, the $d_{(\text{O}\cdots\text{O})}$ distances for the atoms shared by the coordination

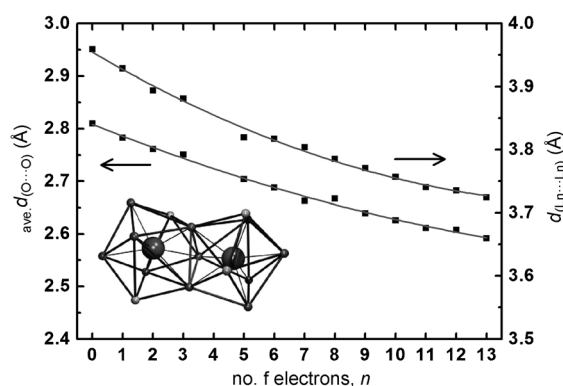


Figure 4. Graphs of Ln···Ln distances and average of various O···O distances (gray in inset) versus the number of 4f electrons (n) for complexes **1** to **13**. The solid lines are best fits (weighted for the Ln···Ln distances) to quadratic functions $F(n) = a + bn + cn^2$, demonstrating that these parameters follow quadratic decays with n . Best-fit parameters: $a = 3.9568(3)$, $b = -0.0285(1)$, and $c = 0.00083(1)$ with $R^2 = 0.9978$; $a = 2.809(4)$, $b = -0.023(1)$, and $c = 0.00050(1)$ with $R^2 = 0.9939$, for $d_{(\text{Ln}\cdots\text{Ln})}$ and average $d_{(\text{O}\cdots\text{O})}$, respectively).

polyhedra of both sites (O3, O8, O13) were analyzed jointly (Figure 4), which also resulted in a quadratic decay. Such observation is the first manifestation of the lanthanide contraction on parameters affected by two lanthanide atoms simultaneously. This could also be probed by plotting the dependence of the Ln···Ln distances on n (Figure 4), which exhibits the same behavior.

Electrospray mass spectrometry (ESI-MS): Electrospray mass spectrograms were recorded for compounds **1** to **15**. They showed several important peaks that correspond to various ligand fragments, whereas weaker signals could be identified that arose from the complexes. The experiments were performed in methanol, in which the system was shown to persist for the time necessary to collect the data (see below). The poor intensity of the latter species versus the fragments of the ligands is not surprising, since unsaturated lanthanide complexes are known to possess weak ESI-MS responses that result from the difficulty of solvated species to transfer to the gas phase.^[40] The ionization of the clusters was achieved after losing the pyridine and H_2O ligands and the NO_3^- group, thus leading to general formulae $[\text{Ln}_2(\text{HL})_2(\text{H}_2\text{L})]^+$. The mass spectrometric study also showed the addition of a second proton atom onto that species, thus leading to $[\text{Ln}_2(\text{HL})(\text{H}_2\text{L})_2]^2+$, or the addition of a sodium ion that substituted a proton, most likely from the H_2L^- moiety, which led to $[\text{Ln}_2(\text{HL})_3] + \text{Na}^+$. Experimental isotope patterns for these species are shown in Figures S4–S18 in the Supporting Information for all complexes reported, thereby confirming the formulation of each system. A representative example of the signal given by these two distinctive fragments is shown in Figure 5 for the case of $[\text{Er}_2(\text{HL})_2(\text{H}_2\text{L})(\text{NO}_3)(\text{py})(\text{H}_2\text{O})]$ (**11**), along with the simulated diagrams. Especially important is the case of compound **14** (Lu), for which no crystal data could be obtained. The existence of the characteristic molecular peaks for this

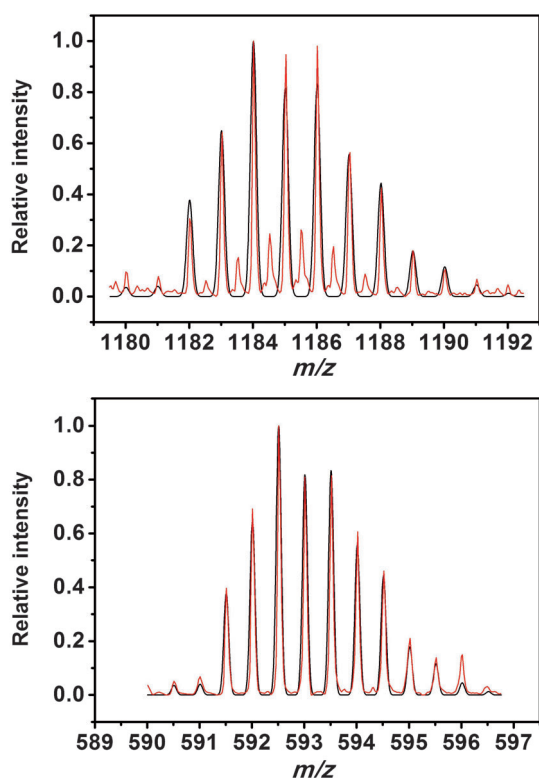


Figure 5. Selected fragments of the mass spectrogram (red lines) of [Er₂(HL)₂(H₂L)(NO₃)(py)(H₂O)] (**11**) as a representative example of the complex series in this work. The simulated signals (black lines) are also represented to show the isotopic distribution. Top: fragment [Ln₂(HL)₂(H₂L)]⁺. Bottom: fragment [Ln₂(HL)(H₂L)₂]²⁺.

complex in the mass spectrometry confirms its successful synthesis, as also shown by infrared spectroscopy and elemental analysis.

Magnetic properties: The large unquenched orbital moment of lanthanide ions converts them into an exquisite tool in molecular magnetism. Recent years have garnered increased interest as a result of the attractive behavior of many Ln^{III} complexes as single-molecule magnets (SMMs), as they exhibit magnetic hysteresis at relatively high temperatures and also high anisotropy barriers.^[10,41–47] The electronic ground state of 4fⁿ ions are determined by electron–electron repulsion and the spin–orbit coupling, usually stronger than the interaction with the crystal field. The latter interaction removes the (2J+1)-fold degeneracy of each multiplet associated with a total angular momentum J, thus leading to a manifold of substates known as Stark levels and to a net magnetic anisotropy. At room temperature, all Stark levels of the ground-state multiplet are usually populated. However, as temperature decreases, the excited sublevels start depopulating, thus leading to a variation of the $\chi_M T$ versus T curve. In a Ln^{III} dinuclear compound, the magnetic response depends not only on this effect but also on the magnetic exchange between both ions. This magnetic exchange is almost always weak, and is thus masked by the depopulation of the Stark levels. However, the case of Gd^{III} is special, since this

lanthanoid has no orbital momentum (L=0), and thus it displays spin-only magnetism that results from a ⁸S_{7/2} state, and a very weak magnetic anisotropy. In our previous work,^[34] the lack of orbital momentum in the related [Gd₂] complex **16** was used to demonstrate the presence of weak antiferromagnetic coupling. Very low-temperature measurements showed also the existence of a finite exchange coupling of comparable magnitude in the complex [Tb₂(HL)₂(H₂L)Cl(py)₂] (**17**).^[36]

In the present work, the magnetic behavior of all nondiamagnetic complexes prepared was investigated through variable-temperature bulk magnetization measurements performed on powdered microcrystalline samples. Figure 6

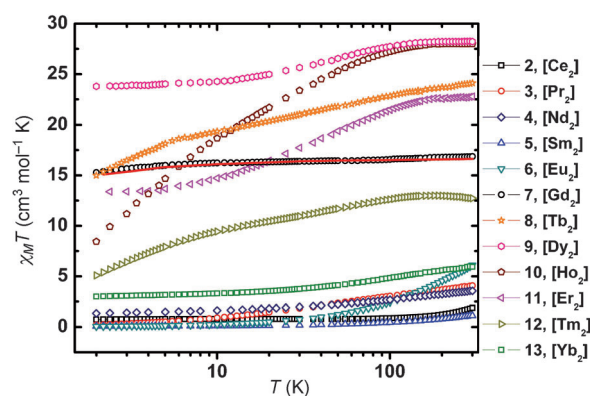


Figure 6. Curves of $\chi_M T$ versus T for compounds **2** to **13**, χ_M being the molar paramagnetic susceptibility per [Ln₂] unit. The full red line represents the best fit of the experimental data for **7** (see text for details).

shows the temperature dependence of $\chi_M T$, χ_M being the molar paramagnetic susceptibility. Experimental $\chi_M T$ values measured at 300 K, as well as the calculated ones considering two isolated Ln^{III} ions in the (2S+1)L_J ground state, are also listed in Table 3. The majority of the measured values at 300 K agree well with those expected at this temperature for two uncoupled metals with all the Stark levels quasi-equally populated. However, complexes **5** (Sm) and **6** (Eu) deviate significantly from this behavior, which confirms the

Table 3. Experimental $\chi_M T$ values for complexes **2–13** at T=300 K and the calculated values corresponding to two isolated Ln^{III} ions in the (2S+1)L_J ground state.

	(2S+1)L _J	g _J	$\chi_M T$ (calcd) ^[a]	$\chi_M T$ (exptl) ^[a]
Ce (2)	² F _{5/2}	6/7	1.60	1.88
Pr (3)	³ H ₄	4/5	3.20	4.07
Nd (4)	⁴ I _{9/2}	8/11	3.28	3.55
Sm (5)	⁶ H _{5/2}	2/7	0.18	1.17
Eu (6)	⁷ F ₀	–	0	3.45
Gd (7)	⁸ S _{7/2}	2	15.76	16.80
Tb (8)	⁷ F ₆	3/2	23.64	24.11
Dy (9)	⁶ H _{15/2}	4/3	28.34	28.22
Ho (10)	⁵ I ₈	5/4	28.14	27.99
Er (11)	⁴ I _{15/2}	6/5	22.96	22.74
Tm (12)	³ H ₆	7/6	14.30	12.72
Yb (13)	² F _{7/2}	8/7	5.14	5.97

[a] In cm³ K⁻¹ mol⁻¹.

influence of low-lying excited multiplets in these metals.^[48] The dependence of the $\chi_M T$ product on temperature provides information on the crystal field and exchange interactions present in each complex. As argued above, complex **7**, with Gd, represents an especially simple situation, free from the contributions of the spin–orbit and crystal-field interactions. In this case, $\chi_M T$ shows a stable value from room temperature down to 40 K. Below this temperature, it gradually decreases, ultimately reaching a value of $15.28 \text{ cm}^3 \text{ K mol}^{-1}$ at 2 K. Since no anisotropic effects can be invoked, this decline can only be ascribed to the presence of weak antiferromagnetic interactions between the two Gd^{III} ions. As mentioned above, an analogous response was found previously for complex **16**.^[34] The $\chi_M T$ versus T curve was modeled using an isotropic spin Hamiltonian ($H = -JS_1S_2$), as well as a temperature-independent paramagnetic (TIP) susceptibility of $6 \times 10^{-4} \text{ cm}^3 \text{ K}^{-1} \text{ mol}^{-1}$.^[49] The best fit was obtained for $J = -0.04(2) \text{ cm}^{-1}$ and $g = 2.05(1)$, which are in agreement with the literature data^[50] and with the values found for **16**.^[34] As expected, the magnetic responses of all the other complexes follow a qualitatively different behavior. For these compounds, $\chi_M T$ begins to decrease at as high as 300 K. As a general rule, this decrease can be attributed to the depopulation of excited Stark sublevels that belong to the ground multiplet of each lanthanide ion. The intramolecular exchange interactions can lead to an additional drop in $\chi_M T$, analogous to that observed for complex **7**. This behavior is clearly observed for complexes **2** (Ce), **8** (Tb), **9** (Dy), **10** (Ho), and **12** (Tm). As T decreases below 300 K, $\chi_M T$ first decreases to an intermediate value, after which a second, faster decline occurs. The first decrease can be attributed to the depopulation of Stark sublevels, whereas the second decline is most likely due to a weak antiferromagnetic coupling between both Ln^{III} ions. For complexes **3** (Pr), **4** (Nd), **11** (Er), and **13** (Yb), these two steps are not as clearly separated, since $\chi_M T$ decreases continuously throughout the whole temperature range. However, both contributions might still be considered.

Photoluminescent properties: Room-temperature absorption spectra of complexes **1** to **15** and of the free ligand H₃L were collected in DMF by using a concentration of 10^{-5} M . A representative spectrum is shown on Figure S19 in the Supporting Information, whereas all the data are listed on Table S4 in the Supporting Information. The suitability of this solvent was examined by performing the absorption measurement on one of the complexes, [Eu₂(HL)₂(H₂L)(NO₃)(py)(H₂O)] (**6**), at various intervals over 24 h (Figure S20 in the Supporting Information). The absorption experienced only a very slow decline, thus demonstrating the sufficient stability of the complexes in this solution during the experiments. Likewise, the spectrum originally collected in MeOH exhibited the same stability. Very similar values in absorption maxima were observed in all systems. Within this family of complexes, going from metal to metal has only minor effects on the intensity and shift of the absorption bands. Above 300 nm, the spectra exhibit a broad absorp-

tion band with λ_{max} in the range from 385 to 387 nm, which is always accompanied by a shoulder of lower intensity between 405 and 408 nm (Figure S19 in the Supporting Information). Both bands are directly related to the ligand (see spectrum of H₃L in Figure S19 in the Supporting Information) and might be attributed to π – π^* transitions as observed in related systems.^[51,52]

A slight redshift in absorption is observed for the complexes with respect to the free ligand, which is indicative of coordination between ligands and metal centers. The steady-state luminescence of **1** to **15** and H₃L were investigated in DMF in the concentration 10^{-5} M . All the systems were recorded in the visible and/or near-IR regions. H₃L exhibits a broad emission band at 388 nm (Figure S21 in the Supporting Information). In turn, all complexes display a single broad emission band in that region while no sharp lanthanide emissions were found. This indicates that, for the complexes, luminescence in this region is exclusively due to the coordinated ligand (Figure S21 in the Supporting Information). On the other hand, only **4** (Nd), **11** (Er), and **13** (Yb) displayed spectra in the near-IR region and showed features that corresponded to metal-based transitions.^[53,54] Figure 7 shows the emission spectra of **4** (Nd), **11** (Er), and **13** (Yb) recorded from 800 to 1600 nm under the excitation of light with $\lambda = 385, 385,$ and 355 nm , respectively. The spectra in all three cases show transitions with precedents in other luminescent Yb, Nd, and Er compounds.^[53,54] Thus, the above-mentioned excitations resulted in narrow emission bands

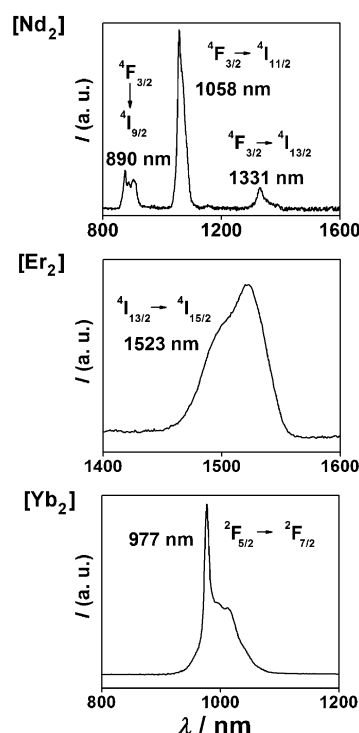


Figure 7. Fluorescence emission spectra of complexes **4** (Nd, top), **11** (Er, middle), and **13** (Yb, bottom) in 10^{-5} M DMF at room temperature, under the excitation of light with $\lambda = 385, 385,$ and 355 nm , respectively. Intensities are normalized. See text for further details.

near 890, 1058, and 1331 nm for **4** (Nd), 1523 nm for **11** (Er), and 977 nm for **13** (Yb). These bands were assigned to the transitions $^4F_{3/2} \rightarrow ^4I_{9/2}$, $^4F_{3/2} \rightarrow ^4I_{11/2}$ (the most intense), and $^4F_{3/2} \rightarrow ^4I_{13/2}$ for the [Nd₂] complex, $^4I_{13/2} \rightarrow ^4I_{15/2}$ for the [Er₂] system, and $^2F_{5/2} \rightarrow ^2F_{7/2}$ for the [Yb₂] complex.^[52–54] Overall, these transitions might be due to an antenna effect that has been well described for other β-diketonate systems, in which effective intramolecular energy transference from the coordinated H₃L ligand (as H₂L[−] and HL[−]) to the central lanthanide would lead to radiative emitting processes.^[55]

Conclusion

The first structurally characterized quasi-complete series of dinuclear lanthanide complexes has been employed for the study of the lanthanide contraction of two metal centers, simultaneously, within two different coordination environments. The quadratic nature of the decay in each site has been seen by analyzing the sum of all Ln–O distances that belong to the partially deprotonated H₃L ligand, and suitably evaluated with Slater's model of the atomic radii. Parameters that affect both Ln^{III} ions, such as Ln···Ln or coordination polyhedra O···O distances shared by both metals, have been demonstrated to follow the quadratic decay due to the contraction as well. The difference between cavity size in both environments is maintained throughout the series as a result of structural constraints imposed by the molecular arrangement. The use of this behavior to design heterometallic dinuclear lanthanide complexes, thus combining two lanthanide ions with different ionic radii, is being investigated.

Experimental Section

[La₂(HL)₂(H₂L)(NO₃)(py)(H₂O)] (1): Method 1: A yellow solution of H₃L (30.0 mg, 0.11 mmol) in pyridine (10 mL) was added into a colorless solution of La(NO₃)₃·6H₂O (30.3 mg, 0.07 mmol) in pyridine (10 mL). The mixture was stirred for 2 h, and the resulting yellow solution was layered with Et₂O. After two weeks, the complex was obtained as a yellow solid (43%, 19.4 mg). Method 2: A yellow solution of H₃L (30.0 mg, 0.11 mmol) in pyridine (10 mL) was added into a colorless solution of La(NO₃)₃·6H₂O (30.3 mg, 0.07 mmol) in pyridine (10 mL). The mixture was stirred for 30 min, when a colorless 0.13 M solution of HNO₃ in MeCN (270 μL, 0.035 mmol) was added dropwise. The reaction was left stirring for 2 h, and the resulting yellow solution was layered with Et₂O. After three weeks, small yellow crystals of **1** were collected (40%, 18.0 mg).

[Ce₂(HL)₂(H₂L)(NO₃)(py)(H₂O)] (2): A yellow solution of H₃L (30.0 mg, 0.11 mmol) in pyridine (10 mL) was added into a colorless solution of Ce(NO₃)₃·6H₂O (30.4 mg, 0.07 mmol) in pyridine (10 mL). The mixture was stirred for 2 h, and the resulting orange solution was layered with Et₂O. After two weeks, the complex was obtained as red crystals (77%, 34.6 mg).

[Pr₂(HL)₂(H₂L)(NO₃)(py)(H₂O)] (3): A yellow solution of H₃L (30.0 mg, 0.11 mmol) in pyridine (10 mL) was added into a light green solution of Pr(NO₃)₃·6H₂O (30.5 mg, 0.07 mmol) in pyridine (10 mL). The mixture was stirred for 2 h, and the resulting yellow solution was layered with Et₂O. After two weeks, the complex was obtained as yellow crystals (87%, 39.1 mg).

[Nd₂(HL)₂(H₂L)(NO₃)(py)(H₂O)] (4): A yellow solution of H₃L (30.0 mg, 0.11 mmol) in pyridine (10 mL) was added into a colorless solution of Nd(NO₃)₃·6H₂O (30.7 mg, 0.07 mmol) in pyridine (10 mL). The mixture was stirred for 2 h, and the resulting yellow solution was layered with toluene. After two weeks, the complex was obtained as yellow crystals (69%, 31.3 mg).

[Sm₂(HL)₂(H₂L)(NO₃)(py)(H₂O)] (5): A yellow solution of H₃L (30.0 mg, 0.11 mmol) in pyridine (10 mL) was added into a colorless solution of Sm(NO₃)₃·6H₂O (31.1 mg, 0.07 mmol) in pyridine (10 mL). The mixture was stirred for 2 h, and the resulting yellow solution was layered with Et₂O. After two weeks, the complex was obtained as yellow crystals (81%, 37.2 mg).

[Eu₂(HL)₂(H₂L)(NO₃)(py)(H₂O)] (6): A yellow solution of H₃L (30.0 mg, 0.11 mmol) in pyridine (10 mL) was added into a colorless solution of Eu(NO₃)₃·5H₂O (30.0 mg, 0.07 mmol) in pyridine (10 mL). The mixture was stirred for 2 h, and the resulting orange solution was layered with Et₂O. After two weeks, the complex was obtained as yellow crystals (91%, 42.0 mg).

[Gd₂(HL)₂(H₂L)(NO₃)(py)(H₂O)] (7): A yellow solution of H₃L (30.0 mg, 0.11 mmol) in pyridine (10 mL) was added into a colorless solution of Gd(NO₃)₃·6H₂O (31.6 mg, 0.07 mmol) in pyridine (10 mL). The mixture was stirred for 2 h, and the resulting yellow solution was layered with Et₂O. After two weeks, the complex was obtained as yellow crystals (90%, 41.8 mg).

[Tb₂(HL)₂(H₂L)(NO₃)(py)(H₂O)] (8): A yellow solution of H₃L (30.0 mg, 0.11 mmol) in pyridine (10 mL) was added into a colorless solution of Tb(NO₃)₃·6H₂O (30.5 mg, 0.07 mmol) in pyridine (10 mL). The mixture was stirred for 2 h, and the resulting yellow solution was layered with Et₂O. After two weeks, the complex was obtained as yellow crystals (66%, 30.7 mg).

[Dy₂(HL)₂(H₂L)(Cl)(py)(H₂O)] (9): A yellow solution of H₃L (30.0 mg, 0.11 mmol) in pyridine (10 mL) was added into a colorless solution of Dy(NO₃)₃·6H₂O (32.0 mg, 0.07 mmol) in pyridine (10 mL). The mixture was stirred for 2 h, and the resulting orange solution was layered with Et₂O. After two weeks, the complex was obtained as yellow crystals (71%, 33.2 mg).

[Ho₂(HL)₂(H₂L)(NO₃)(py)(H₂O)] (10): A yellow solution of H₃L (30.0 mg, 0.11 mmol) in pyridine (10 mL) was added into a colorless solution of Ho(NO₃)₃·5H₂O (30.8 mg, 0.07 mmol) in pyridine (10 mL). The mixture was stirred for 2 h, and the resulting yellow solution was layered with Et₂O. After two weeks, the complex was obtained as yellow crystals (75%, 35.2 mg).

[Er₂(HL)₂(H₂L)(NO₃)(py)(H₂O)] (11): A yellow solution of H₃L (30.0 mg, 0.11 mmol) in pyridine (10 mL) was added into a colorless solution of Er(NO₃)₃·5H₂O (31.0 mg, 0.07 mmol) in pyridine (10 mL). The mixture was stirred for 2 h, and the resulting orange solution was layered with toluene. After two weeks, the complex was obtained as yellow crystals (59%, 27.8 mg).

[Tm₂(HL)₂(H₂L)(NO₃)(py)(H₂O)] (12): A yellow solution of H₃L (30.0 mg, 0.11 mmol) in pyridine (10 mL) was added into a colorless solution of Tm(NO₃)₃·5H₂O (31.2 mg, 0.07 mmol) in pyridine (10 mL). The mixture was stirred for 2 h, and the resulting yellow solution was layered with ether. After two weeks, the complex was obtained as yellow crystals (15%, 7.9 mg).

[Yb₂(HL)₂(H₂L)(NO₃)(py)(H₂O)] (13): A yellow solution of H₃L (30.0 mg, 0.11 mmol) in pyridine (8 mL) was added into a colorless solution of Yb(NO₃)₃·5H₂O (31.1 mg, 0.07 mmol) in pyridine (8 mL). After addition of 69% HNO₃ (6.81 μL, 0.11 mmol), the mixture was stirred for 1 h, and the resulting yellow solution was layered with hexane. After four weeks, small orange crystals of **13** were collected (7%, 3.0 mg).

[Lu₂(HL)₂(H₂L)(NO₃)(py)(H₂O)] (14): A yellow solution of H₃L (30.0 mg, 0.11 mmol) in pyridine (10 mL) was added into a colorless solution of Lu(NO₃)₃·H₂O (25.3 mg, 0.07 mmol) in pyridine (10 mL). The mixture was stirred for 2 h, and the resulting orange solution was layered with Et₂O. After two weeks, the complex was obtained as an orange solid (23%, 10.9 mg).

[Y₂(HL)₂(H₂L)(NO₃)(py)(H₂O)] (15): A yellow solution of H₃L (30.0 mg, 0.11 mmol) in pyridine (15 mL) was added into a colorless solution of Y(NO₃)₃·6H₂O (26.9 mg, 0.07 mmol) in pyridine (15 mL). The mixture was stirred under reflux for 2 h, and then cooled to room temperature. The resulting orange solution was layered with ether. After two weeks, the complex was obtained as orange crystals (39%, 16.9 mg).

Physical measurements: Variable-temperature magnetic susceptibility data for compounds **2** to **12** and **14** were obtained on microcrystalline samples by using a Quantum Design MPMS-XL SQUID magnetometer either at the “Unitat de Mesures Magnètiques” of the Universitat de Barcelona or at the SAI Physical Measurements of the University of Zaragoza. Pascal’s constants were used to estimate diamagnetic corrections to the molar paramagnetic susceptibility, and a correction was applied for the sample holder. IR spectra were recorded on KBr pellets, in the range 4000–400 cm⁻¹, using a Thermo Nicolet Avatar 330 FTIR spectrometer. Elemental analyses were performed using a Perkin–Elmer Series II CHNS/O Analyzer 2400 at the Servei de Microanàlisi of the CSIC, Barcelona. Electronic absorption spectra were recorded with 1 nm resolution using a Varian Cary 100 UV/Vis spectrophotometer in DMF at room temperature (*c* = 10⁻⁵ M). Fluorescence emission spectra were carried out using Horiba Jobin–Yvon SPEX Nanolog-TM and Cary Eclipse spectrofluorimeters. The slits used were of 5 nm for [Nd₂] (**4**) and [Yb₂] (**14**) and 10 nm for [Er₂] (**11**). Positive-ion ESI mass spectrometry experiments were performed using a LC/MSD-TOF (Agilent Technologies) with a dual source equipped with a lock spray for internal reference introduction at the Unitat d’Espectrometria de Masses (SSR) of the University of Barcelona. The experimental parameters were capillary voltage 4 kV, gas temperature 325 °C, nebulizing gas pressure 15 psi, drying gas flow 7.0 L min⁻¹, and fragmentor voltage ranging from 175 to 250 V. Internal reference masses were *m/z* 121.05087 (purine) or 922.00979 (HP-0921). Samples (microliters) were introduced into the source using an HPLC system (Agilent 1100), using a mixture of H₂O/CH₃CN (1:1) as eluent (200 μL min⁻¹).

X-ray crystallography: Crystals systematically suffer from deterioration of crystallinity once out of their mother liquor, likely due to lattice solvent loss. Single crystals were therefore selected and mounted directly from their mother liquor using the oil-drop method and mounted as fast as possible into the cold N₂ stream on the goniometer. Data for compounds **1-5** py, **4-6** py, and **13-6** py were collected with MoK_α radiation (λ = 0.71073 Å) using a Bruker APEX II QUAZAR diffractometer equipped with a microfocus multilayer monochromator at 100 K. Data for compounds **2-6** py, **3-6** py, **5-5** py·H₂O, **6-5** py·H₂O, **8-5** py, **11-5** py, and **15-4** py were collected at 100 K (150 K for **5-5** py·H₂O) using a Bruker APEX II CCD diffractometer on the Advanced Light Source beamline 11.3.1 at Lawrence Berkeley National Laboratory, from a silicon 111 monochromator (λ = 0.7749 Å). Data reduction and absorption corrections were performed with SAINT and SADABS.^[56] Data for compounds **7-5** py, **9-5** py, **10-5** py, and **12-5** py·Et₂O were obtained at 150 K using an Oxford Diffraction Excalibur diffractometer with enhanced MoK_α radiation (λ = 0.71073 Å) at the X-ray diffraction and Fluorescence Analysis Service of the University of Zaragoza. Cell refinement, data reduction, and absorption corrections were performed with the CrysAlisPro suite.^[57] All structures were solved and refined on *F*² with the SHELXTL suite.^[58,59] All non-hydrogen atoms were refined anisotropically. Hydrogen atoms were placed geometrically on their carrier atom and refined with a riding model. In all cases, displacement parameters restraints were used to refine some of the lattice solvent molecules. For **1-5** py, **4-6** py, **7-5** py, **8-5** py, **9-5** py, **10-5** py, **11-5** py, and **15-4** py void space with only diffuse electron density remaining at the end of the refinement were analyzed and taken into account with SQUEEZE as implemented in the PLATON package.^[60,61] Crystallographic and refinement parameters are summarized in Table 1. Selected bond lengths and angles are given in Table 2 and Table S1 in the Supporting Information.

CCDC-915325 (**1**), 915326 (**2**), 915327 (**3**), 915328 (**4**), 915329 (**5**), 915330 (**6**), 915331 (**7**), 915332 (**8**), 915333 (**9**), 915334 (**10**), 915335 (**11**), 915336 (**12**), 918743 (**13**), and 915337 (**15**) contain the supplementary crystallographic data for this paper. These data can be obtained free of charge

from The Cambridge Crystallographic Data Centre via www.ccdc.cam.ac.uk/data_request/cif.

Acknowledgements

G.A. thanks the Generalitat de Catalunya for the prize ICREA Academia 2008 and the ERC for a starting grant (258060 FuncMolQIP). The authors thank the Spanish MCI through CTQ2009-06959 (N.A.A., D.A., V.V., L.B., and G.A.), and MAT2011-24284 (O.R.). The Advanced Light Source is supported by the Director, Office of Science, Office of Basic Energy Sciences of the U.S. Department of Energy under contract no. DE-AC02-05CH11231.

- [1] S. V. Eliseeva, J. C. G. Bunzli, *New J. Chem.* **2011**, *35*, 1165–1176.
- [2] K. Binnemans, *Chem. Rev.* **2009**, *109*, 4283–4374.
- [3] K. Kuriki, Y. Koike, Y. Okamoto, *Chem. Rev.* **2002**, *102*, 2347–2356.
- [4] Y. Hasegawa, Y. Wada, S. Yanagida, H. Kawai, N. Yasuda, T. Nagamura, *Appl. Phys. Lett.* **2003**, *83*, 3599–3601.
- [5] A. de Bettencourt-Dias, *Dalton Trans.* **2007**, 2229–2241.
- [6] B. S. Richards, *Sol. Energy Mater. Sol. Cells* **2006**, *90*, 1189–1207.
- [7] C. Benelli, D. Gatteschi, *Chem. Rev.* **2002**, *102*, 2369–2387.
- [8] G. Aromí, E. K. Brechin, *Struct. Bonding (Berlin)* **2006**, *122*, 1–67.
- [9] J. D. Rinehart, J. R. Long, *Chem. Sci.* **2011**, *2*, 2078–2085.
- [10] N. Ishikawa, M. Sugita, T. Ishikawa, S. Koshihara, Y. Kaizu, *J. Am. Chem. Soc.* **2003**, *125*, 8694–8695.
- [11] L. Ungur, L. F. Chibotaru, *Phys. Chem. Chem. Phys.* **2011**, *13*, 20086–20090.
- [12] G. Cucinotta, M. Perfetti, J. Luzón, M. Etienne, P.-E. Car, A. Canechi, G. Calvez, K. Bernot, R. Sessoli, *Angew. Chem. Int. Ed.* **2012**, *51*, 1606–1610.
- [13] J. Luzón, R. Sessoli, *Dalton Trans.* **2012**, *41*, 13556–13567.
- [14] L. Sorace, C. Benelli, D. Gatteschi, *Chem. Soc. Rev.* **2011**, *40*, 3092–3104.
- [15] P. D’Angelo, A. Zitolo, V. Migliorati, G. Chillemi, M. Duvaill, P. Vitorge, S. Abadie, R. Spezia, *Inorg. Chem.* **2011**, *50*, 4572–4579.
- [16] A. Bowden, S. J. Coles, M. B. Pitak, A. W. G. Platt, *Inorg. Chem.* **2012**, *51*, 4379–4389.
- [17] Y. Fukuda, A. Nakao, K. Hayashi, *J. Chem. Soc. Dalton Trans.* **2002**, 527–533.
- [18] J. Cepeda, R. Balda, G. Beobide, O. Castillo, J. Fernández, A. Luque, S. Pérez-Yáñez, P. Román, D. Vallejo-Sánchez, *Inorg. Chem.* **2011**, *50*, 8437–8451.
- [19] Z. He, E.-Q. Gao, Z.-M. Wang, C.-H. Yan, M. Kurmoo, *Inorg. Chem.* **2005**, *44*, 862–874.
- [20] G.-L. Zhuang, X.-J. Kong, L.-S. Long, R.-B. Huang, L.-S. Zheng, *CrystEngComm* **2010**, *12*, 2691–2694.
- [21] P. V. Bernhardt, B. M. Flanagan, M. J. Riley, *Aust. J. Chem.* **2001**, *54*, 229–232.
- [22] P. V. Bernhardt, B. M. Flanagan, M. J. Riley, *Aust. J. Chem.* **2000**, *53*, 229–231.
- [23] K. Matsumoto, K. Suzuki, T. Tsukuda, T. Tsubomura, *Inorg. Chem.* **2010**, *49*, 4717–4719.
- [24] M. Seitz, A. G. Oliver, K. N. Raymond, *J. Am. Chem. Soc.* **2007**, *129*, 11153–11160.
- [25] A. Chatterjee, E. N. Maslen, K. J. Watson, *Acta Crystallogr. Sect. B* **1988**, *44*, 381–386.
- [26] I. Persson, P. D’Angelo, S. De Panfilis, M. Sandstrom, L. Eriksson, *Chem. Eur. J.* **2008**, *14*, 3056–3066.
- [27] E. A. Quadrelli, *Inorg. Chem.* **2002**, *41*, 167–169.
- [28] E. Clementi, D. L. Raimondi, W. P. Reinhardt, *J. Chem. Phys.* **1967**, *47*, 1300–1307.
- [29] J. C. Slater, *Phys. Rev.* **1930**, *36*, 57–64.
- [30] J. Chakraborty, A. Ray, G. Pilet, G. Chastanet, D. Luneau, R. F. Ziessel, L. J. Charbonniere, L. Carrella, E. Rentschler, M. S. El Fallah, S. Mitra, *Dalton Trans.* **2009**, 10263–10272.

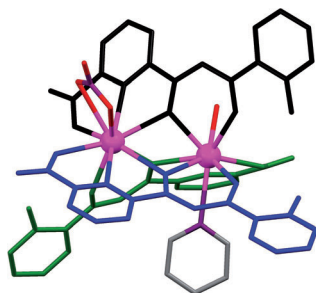
- [31] P.-H. Lin, M. Leclere, J. Long, T. J. Burchell, I. Korobkov, R. Clérac, M. Murugesu, *Dalton Trans.* **2010**, 39, 5698–5704.
- [32] L. S. Natrajan, P. L. Timmins, M. Lunn, S. L. Heath, *Inorg. Chem.* **2007**, *46*, 10877–10886.
- [33] J.-X. Xu, Y. Ma, D.-Z. Liao, G.-F. Xu, J. Tang, C. Wang, N. Zhou, S.-P. Yan, P. Cheng, L.-C. Li, *Inorg. Chem.* **2009**, *48*, 8890–8896.
- [34] D. Aguilà, L. A. Barrios, F. Luis, A. Repollés, O. Roubeau, S. J. Teat, G. Aromí, *Inorg. Chem.* **2010**, *49*, 6784–6786.
- [35] G. Aromí, D. Aguilà, P. Gamez, F. Luis, O. Roubeau, *Chem. Soc. Rev.* **2012**, *41*, 537–546.
- [36] F. Luis, A. Repollés, M. J. Martínez-Pérez, D. Aguilà, O. Roubeau, D. Zueco, P. J. Alonso, M. Evangelisti, A. Camón, J. Sesé, L. A. Barrios, G. Aromí, *Phys. Rev. Lett.* **2011**, *107*, 117203.
- [37] M. Estrader, J. Ribas, V. Tangoulis, X. Solans, M. Font-Bardía, M. Maestro, C. Díaz, *Inorg. Chem.* **2006**, *45*, 8239–8250.
- [38] A. Ruiz-Martínez, S. Alvarez, *Chem. Eur. J.* **2009**, *15*, 7470–7480.
- [39] A. Ruiz-Martínez, D. Casanova, S. Alvarez, *Chem. Eur. J.* **2008**, *14*, 1291–1303.
- [40] C. Piguet, J.-C. G. Bünzli, G. Bernardinelli, G. Hopfgartner, S. Petoud, O. Schaad, *J. Am. Chem. Soc.* **1996**, *118*, 6681–6697.
- [41] M. T. Gamer, Y. Lan, P. W. Roesky, A. K. Powell, R. Clérac, *Inorg. Chem.* **2008**, *47*, 6581–6583.
- [42] Y.-N. Guo, G.-F. Xu, P. Gamez, L. Zhao, S.-Y. Lin, R. Deng, J. Tang, H.-J. Zhang, *J. Am. Chem. Soc.* **2010**, *132*, 8538–8539.
- [43] S.-D. Jiang, S.-S. Liu, L.-N. Zhou, B.-W. Wang, Z.-M. Wang, S. Gao, *Inorg. Chem.* **2012**, *51*, 3079–3087.
- [44] P.-H. Lin, T. J. Burchell, R. Clérac, M. Murugesu, *Angew. Chem.* **2008**, *120*, 8980–8983; *Angew. Chem. Int. Ed.* **2008**, *47*, 8848–8851.
- [45] P.-H. Lin, T. J. Burchell, L. Ungur, L. F. Chibotaru, W. Wernsdorfer, M. Murugesu, *Angew. Chem.* **2009**, *121*, 9653–9656; *Angew. Chem. Int. Ed.* **2009**, *48*, 9489–9492.
- [46] J. D. Rinehart, M. Fang, W. J. Evans, J. R. Long, *Nat. Chem.* **2011**, *3*, 538–542.
- [47] R. Sessoli, A. K. Powell, *Coord. Chem. Rev.* **2009**, *253*, 2328–2341.
- [48] *Spectra and Energy Levels of Rare Earth Ions in Crystals* (Ed: G. H. Dieke), Wiley, New York (USA), **1968**.
- [49] A. Panagiotopoulos, T. F. Zafiroopoulos, S. P. Perlepes, E. Bakalbassis, I. Masson-Ramade, O. Kahn, A. Terzis, C. P. Raptopoulou, *Inorg. Chem.* **1995**, *34*, 4918–4920.
- [50] L. E. Roy, T. Hughbanks, *J. Am. Chem. Soc.* **2006**, *128*, 568–575.
- [51] Y. Luo, B. Chen, W. Wu, X. Yu, Q. Yan, Q. Zhang, *J. Lumin.* **2009**, *129*, 1309–1313.
- [52] A. P. Bassett, S. W. Magennis, P. B. Glover, D. J. Lewis, N. Spencer, S. Parsons, R. M. Williams, L. De Cola, Z. Pikramenou, *J. Am. Chem. Soc.* **2004**, *126*, 9413–9424.
- [53] N. M. Shavaleev, G. Accorsi, D. Virgili, Z. e. R. Bell, T. Lazarides, G. Calogero, N. Armaroli, M. D. Ward, *Inorg. Chem.* **2005**, *44*, 61–72.
- [54] N. M. Shavaleev, R. Scopelliti, F. Gumy, J.-C. G. Bünzli, *Inorg. Chem.* **2009**, *48*, 2908–2918.
- [55] K. Binnemans, in *Handbook on the Physics and Chemistry of Rare Earths, Vol. 35*, Elsevier (Amsterdam), **2005**, pp. 107–272.
- [56] SAINT and SADABS, Bruker AXS Inc., Madison, Wisconsin, USA.
- [57] CrysAlis PRO, Agilent Technologies, Yarnton, UK.
- [58] G. M. Sheldrick, *Acta Crystallogr. Sect. A* **2008**, *64*, 112–122.
- [59] G. M. Sheldrick, SHELXTL, Bruker AXS Inc., Madison, Wisconsin, USA.
- [60] A. L. Spek, PLATON, A Multipurpose Crystallographic Tool, Utrecht University, Utrecht (The Netherlands), **2008**.
- [61] A. L. Spek, *J. Appl. Crystallogr.* **2003**, *36*, 7–13.

Received: December 13, 2012
Published online: ■■■, 0000

Lanthanides

*D. Aguilà, L. A. Barrios, V. Velasco,
L. Arnedo, N. Aliaga-Alcalde,
M. Menelaou, S. J. Teat, O. Roubeau,
F. Luis, G. Aromí** ■■■■-■■■■

 **Lanthanide Contraction within a Series of Asymmetric Dinuclear [Ln₂] Complexes**



Contractual obligation: The quadratic decay of the lanthanide contraction is manifested by using, for the first time, a quasi-isostructural series of dinuclear asymmetric complexes (see figure). Crystallographic parameters of a total of 13 structures have been analyzed to confirm this trend, which also is observed for parameters that receive a simultaneous contribution from two metals.